Inorganic Chemistry
Article
pubs.acs.org/IC

Multichromophoric Arrays Arranged around a Triptycene Scaffold: Synthesis and Photophysics

Thomas Bura,[†] Maria Pia Gullo,[‡] Barbara Ventura,[‡] Andrea Barbieri,[*,‡] and Raymond Ziessel[*,†]

[†]Laboratoire de Chimie Organique et Spectroscopies Avancées (ICPEES-LCOSA), ECPM, UMR 7515 au CNRS, 25 rue Becquerel, 67087 Strasbourg, Cedex 02, France

[‡]Istituto per la Sintesi Organica e la Fotoreattività (ISOF), Consiglio Nazionale delle Ricerche (CNR), Via P. Gobetti 101, 40129 Bologna BO, Italy

Supporting Information

ABSTRACT: Here we report on the synthesis, characterization, and photophysics of multichromophoric arrays based on a triptycene scaffold that acts as a bridging ligand for Ir(III) and Os(II) satellite active components. The triptycene scaffold not only furnishes a rigid star-shaped 3D displacement of the metallic units in space but also plays an active role in the energy cascade. The transition metal complexes have been designed in order to display an ideal cascade in their lowest excited state energy levels. For this purpose, a novel Ir(III) complex containing two dbpz (dibenzo[*a*,*c*]phenazine) ligands (**Ir**) has been synthesized. The key step in the synthesis of the array was the final cross-coupling between the mixed complex **IrF−Os** and **Ir**, providing the target heterotrinuclear complex **IrF−Ir−Os**. The photophysical properties of models confirmed the appropriate energy displacement of the single chosen active units, in the order triptycene > **IrF** > **Ir** > **Os**, and fast and efficient energy transfer processes leading to the final population of the Os-based triplet level have been evidenced. The reported arrays can be considered as efficient antenna systems with an absorption range extending up to 700 nm, where the triptycene bridging ligand provides both a structural and a photophysical function.

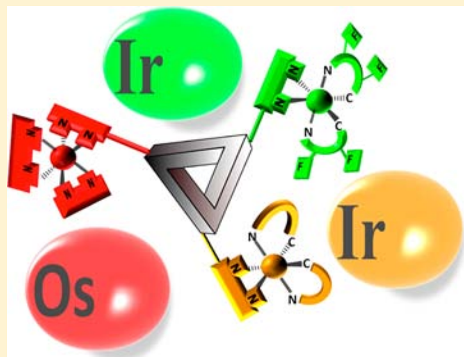

■ INTRODUCTION

Luminescent transition metal complexes (e.g., Ru, Os, Ir, Pt) have attracted attention by many research groups motivated by their exceptional photostability, long excited state lifetimes, and redox activity in the ground and exited states.[1−3] Several potential applications emerge from these studies propelled by the need for the following: (i) models in artificial photosynthesis,[4] (ii) new photocatalysts,[5] (iii) sensors,[6] and (iv) photosensitizers for solar cells.[7] A plethora of complexes were investigated and organized in 1D, 2D, or 3D molecular structures.[8] The last category is less-studied, and only a few examples of phosphorescent complexes based on 3D molecular frameworks (e.g., fullerenes,[9] dendrimers,[10] polymers[11]) have been studied so far. Triptycene, the simplest member of the iptycene family, is a saturated 3D scaffold bearing three arene planes joined together by a [2.2.2]bicyclic ring system.[12] The three rings can be easily and selectively functionalized by three reactive groups in a specific configuration.[13] This situation prompts us to use 2,6,14-trisubstituted triptycene[14] as a preorganized platform to link various phosphorescent Ir and Os modules to create a situation where energy transfer from one module to the other is effective. Such 3D molecular designed multimetallic complexes based on triptycene have never been investigated so far. We here fill the gap and introduce various phosphorescent metallic centers [Ir(III) and Os(II)] to promote cascade energy transfer from the localized triplet states.

From a more general viewpoint, triptycene has been used because of its paddlewheel shape in supramolecular chemistry as a rotor[14] or stator,[15] components in nanodevices, in the construction of host−guest complexes,[16] as molecular cages[17] and chelating ligands in coordination chemistry, as a structure capable of stabilizing sterically bended complexes[18] and highly reactive intermediates in catalytic processes,[19] and in electrophosphorescence.[20] Furthermore, electron and energy transfer in rigid triptycene−bipyridine metal complexes[21] and in porphyrin-based dyads and triads for charge separation[22] has also been investigated. Studies on triptycene-bridged donor/acceptor systems have demonstrated that electronic interactions are occurring through the σ-bridged system,[23] but no homoconjugation effect is present in π-conjugated oligomers.[24]

In the field of polymers, triptycene is credited with improving the mechanical properties of the polymeric network and also the large internal free volume providing large porosity for gas absorption.[25] Interestingly, this large free volume inherent to the triptycene scaffold allows isolation of the polymer backbones resulting in enhanced photoluminescence stability and quantum yields due to the reduction of the interchain

Received: April 2, 2013
Published: July 19, 2013

 © 2013 American Chemical Society

Chart 1. Schematic Representation of the Triptycene Metal-Based Scaffoldings

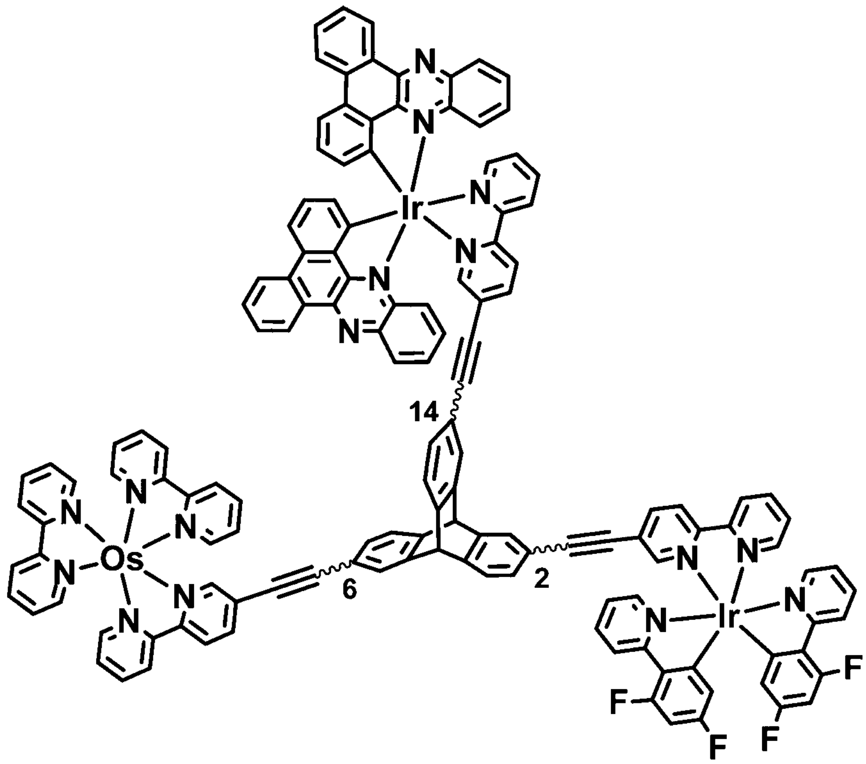

excimer/exciplex formation.[26] Likewise, the 3D shape of triptycene has been exploited to achieve liquid crystal alignment.[27] Herein, we use triptycene as a 3D platform to link two kinds of Ir complexes displaying different energy levels and an Os-bipyridine subunit as the final energy acceptor to promote energy concentration by cascade energy transfer events (Chart 1).

EXPERIMENTAL SECTION

For general methods, starting materials, and photophysical measurements, see Supporting Information. Note that all ligands and complexes described in this Article and in schemes were prepared as mixtures of regioisomers.

Preparation and Characterization. *Compounds L1 and L2.* In a Schlenk tube, compounds **1** (100 mg, 0.158 mmol) and 5-ethynyl-2,2′-bipyridine (e-bipy) (29 mg, 0.158 mmol) were dissolved in a mixture of THF (5 mL) and triethylamine (2 mL). Argon was bubbled through the mixture for 30 min, then $[Pd(PPh_3)_2Cl_2]$ (12 mg) and CuI (3 mg) were added, and the mixture was stirred at room temperature for 1 day. The reaction mixture was extracted with CH_2Cl_2. The organic layer was washed three times with water and dried over absorbent cotton, and the solvent was evaporated under reduced pressure. The crude was purified by column chromatography on alumina eluted with a mixture of CH_2Cl_2/petroleum ether (20/80) and afforded compound **L1** (46 mg, 42%) and **L2** (20 mg, 18%) as a white powder. **L1** ^{1}H NMR ($(CD_3)_2CO$, 300 MHz): δ 5.73 (s, 2H), 7.28−7.33 (m, 3H), 7.40−7.43 (m, 3H), 7.54 (dd, 2H, ^3J = 7.6 Hz, ^4J =2.64 Hz), 7.85−7.95 (m, 3H), 8.01 (d, 1H, ^3J =8.3 Hz), 8.49−8.51 (m, 2H), 8.68 (s broad, 1H), 8.78 (s broad 1H). ^{13}C NMR ($CDCl_3$, 200 MHz): δ 52.8, 53.0, 86.1, 90.5, 93.6, 120.0, 124.1, 124.2, 125.7, 127.1, 128.5, 128.7, 129.5, 132.1, 132.3, 132.9,134.7, 137.2, 139.5, 144.0, 144.4, 144.6, 144.7, 144.9, 146.5, 146.7, 146.8. EI-MS 683.2 ([M], 100). Anal. Calcd for $C_{32}H_{18}I_2N_2$ (M_r = 684.31): C, 56.17; H, 2.65; N, 4.09. Found: C, 56.35; H, 2.77; N, 4.18. **L2** ^{1}H NMR ($(CD_3)_2CO$, 300 MHz): 5.83 (s, 2H), 7.31−7.47 (m, 6H), 7.57−7.67 (m, 2H), 7.74 (s, 2H), 7.90−7.96 (m, 3H), 8.02 (dd, 2H, ^3J =8.26 Hz, ^4J =2.31 Hz), 8.46−8.52 (m, 4H), 8.69 (d, 2H, ^3J =4.9 Hz), 8.78 (s, 2H). ^{13}C NMR ($(CD_3)_2CO$, 200 MHz): 53.3, 53.4, 86.5, 90.7, 94.2, 120.4, 120.9, 121.1, 121.7, 125.1, 125.2, 125.3, 126.9, 127.8, 129.3, 130.1, 132.5, 132.7, 133.8, 135.4, 137.9, 140.1, 145.7, 145.9, 146.2, 146.4, 146.7, 148.3, 150.3, 152.3, 155.8, 156.1. EI-MS *m/z*: 735.5 ([M], 100). Anal. Calcd for $C_{44}H_{25}IN_4$ (M_r = 736.6): C, 71.74; H, 3.42; N, 7.61. Found: C, 71.54; H, 3.54; N, 7.54.

Compound L2′. In a Schlenk tube, compounds **L2** (85 mg, 0.115 mmol) and propargylic alcohol (20 mg, 0.23 mmol) were dissolved in a mixture of THF (6 mL) and triethylamine (3 mL). Argon was bubbled through the mixture for 30 min, then $[Pd(PPh_3)_2Cl_2]$ (10 mg) and CuI (3 mg) were added, and the mixture was stirred at room temperature for 1 day. The reaction mixture was extracted with CH_2Cl_2. The organic layer was washed three times with water and dried over absorbent cotton, and the solvent was evaporated under reduced pressure. The crude was purified by column chromatography on silica gel eluted with a mixture of CH_2Cl_2/petroleum ether/Et_3N (40/48/2) and afforded compound **L2′** as a white powder (82 mg, 82%). ^{1}H NMR ($(CD_3)_2CO$, 300 MHz): δ 1.50 (s, 6H), 5.82 (s, 1H), 5.83 (s, 1H), 7.11 (dd, 1H, ^3J =7.6 Hz, ^4J =1.32 Hz), 7.32 (dd, 2H, ^3J =7.6 Hz, ^4J =1.32 Hz), 7.40−7.44 (m, 2H), 7.49−7.60 (m, 4H), 7.72−7.73 (m, 2H), 7.93 (dt, 2H, ^3J =7.6 Hz, ^4J =1.65 Hz), 8.02 (dd, 2H, ^3J =8.25 Hz, ^4J =2.31 Hz), 8.46−8.51 (m, 4H), 8.68 (d, 2H, ^3J =4.95 Hz), 8.78 (d, 2H, ^4J =1.32 Hz). ^{13}C NMR ($(CD_3)_2CO$, 200 MHz): δ 53.6, 53.7, 81.5, 86.4, 94.2, 95.6, 120.4, 120.9, 121.1, 121.4, 121.7, 124.9, 125.1, 125.2, 127.8, 129.7, 130.1, 137.9, 140.1, 145.5, 145.6, 145.8, 146.2, 146.3, 146.7, 150.3, 152.3, 155.8, 156.1. EI-MS *m/z*: 692.2 ([M], 100). Anal. Calcd for $C_{49}H_{32}N_4O$ (*Mr* = 692.8): C, 84.95; H, 4.66; N, 8.09. Found: C, 84.74; H, 4.34; N, 7.84.

Compound L2″. In a round-bottom flask with benzene (10 mL), compound **L2′** (80 mg, 0.115 mmol) and NaOH (46 mg, 1.15 mmol) were added. The reaction was agitated for 2 h at room temperature. Then, the solvent was evaporated to dryness. The crude was purified by column chromatography on alumina, eluted with CH_2Cl_2 and afforded **L2″** as a white powder (65 mg, 90%). ^{1}H NMR ($(CD_3)_2CO$, 300 MHz): δ 3.56 (s, 1H), 5.82 (s, 1H), 5.83 (s, 1H), 7.22 (dd, 2H, ^3J =7.6 Hz, ^4J =1.32 Hz), 7.31 (dd, 2H, ^3J =7.6 Hz, ^4J =1.32 Hz), 7.38−7.42 (m, 2H), 7.51−7.59 (m, 3H), 7.62−7.64 (m, 1H), 7.72 (s, 1H), 7.91 (dt, 2H, ^3J =7.75 Hz, ^4J =1.32 Hz), 8.01 (dd, 2H, ^3J =8.25 Hz, ^4J

=2.31 Hz), 8.46−8.51 (m, 4H), 8.68 (d, 2H, ^3J =4.3 Hz), 8.78 (d, 2H, ^4J =1.32 Hz). ^{13}C NMR (($CD_3)_2$CO, 200 MHz): δ 53.6, 53.7, 78.5, 84.2, 86.5, 94.2, 120.3, 120.4, 120.9, 121.1, 121.8, 125.0, 125.1, 125.2, 128.2, 130.1, 130.4, 137.8, 140.1, 145.9, 146.1, 146.3, 146.6, 150.2, 152.3, 155.7, 156.1. EI-MS m/z: 634.2 ([M], 100). Anal. Calcd for $C_{46}H_{26}N_4$ (Mr = 634.73): C, 87.04; H, 4.13; N, 8.83. Found: C, 86.88; H, 4.24; N, 8.65.

*Complex **Os−L2**.* Ligand **L2** (60 mg, 0.081 mmol) and complex **C** [Os(bpy)$_2$Cl$_2$] (34 mg, 0.057 mmol) were suspended in ethyl alcohol (10 mL) in a Teflon reactor. The mixture was irradiated with microwaves (1200 W, 180 °C) for 1 h. The solvent was evaporated to dryness. The residue was dissolved in DMF (1 mL) and dropwise added through a pad of Celite into an aqueous solution of KPF_6 (500 mg in 20 mL water). The precipitate was collected on paper and washed with water (3 × 100 mL). The target compound was isolated from the remaining starting material and the bimetallic side product by column chromatography on aluminum oxide eluting with CH_2Cl_2/MeOH (v/v = 100/0 to 96/4) to afford 35 mg (40%) of **Os−L2** black crystals after recrystallization from dichloromethane/diethylether. ^{1}H NMR (($CD_3)_2$CO, 400 MHz): δ 5.78 (s, 1H), 5.83 (s, 1H), 7.16 (d, 1H, ^3J =7.8 Hz), 7.31−7.35 (m, 2H), 7.43−7.51 (m, 10H), 7.70−7.71 (m, 1H), 7.87−8.06 (m, 14H), 8.11 (d, 1H, ^3J =5.3 Hz), 8.46−8.51 (m, 2H), 8.70−8.81 (m, 8H). ESI-MS m/z: 1385.1 ([M − PF_6]$^+$, 100). Anal. Calcd for $C_{64}H_{41}IN_8Os(PF_6)_2$ (Mr = 1529.13): C, 50.27; H, 2.70; N, 7.33. Found: C, 50.42; H, 2.94; N, 7.47.

*Complex **IrF**.* The dimeric complex **B** [**Ir(dfppy)$_2$Cl$_2$**] (50 mg, 0.042 mmol) was dissolved in dichloromethane (3 mL) and methanol (3 mL), and 5-ethynyl-2,2′-bipyridine (16 mg, 0.088 mmol) was added as a solid. The mixture was heated at 60 °C during the night. The solution was cooled to room temperature and the solvent evaporated to dryness. The residue was dissolved in DMF (1 mL) and dropwise added through a pad of Celite into an aqueous solution of KPF_6 (500 mg in 20 mL of water). The precipitate was collected on paper and washed with water (3 × 100 mL). The complex was dried in air and was purified by column chromatography on alumina. The desired complex was eluted with a gradient of methanol (0−1 %) in dichloromethane as mobile phase. The analytically pure complex **IrF** was obtained as yellow powder by recrystallization in a mixture of dichloromethane/diethylether (30 mg, 80%). ^{1}H NMR (($CD_3)_2$CO, 300 MHz): δ 4.2 (s, 1H), 5.76 (dd, 1H ^3J =8.6 Hz, ^4J =2.31 Hz), 5.84 (dd, 1H ^3J =8.6 Hz, ^4J =2.30 Hz), 6.74−6.81 (m, 2H), 7.21−7.27 (m, 2H), 7.75−7.80 (m, 1H), 7.93 (d, 1H, ^3J =5.3 Hz), 8.04−8.10 (m, 3H), 8.17 (d, 1H, ^3J =1.7 Hz), 8.23 (d, 1H, ^3J =5.3 Hz), 8.34−8.40 (m, 4H), 8.88 (dd, 2H, ^3J =8.6 Hz, ^4J =2.3 Hz). EI-MS m/z: 753.1 ([M − PF_6]$^+$, 100). Anal. Calcd for $C_{34}H_{20}F_4IrN_4(PF_6)$ (Mr = 897.7): C, 45.49; H, 2.25; N, 6.24. Found: C, 45.24; H, 1.95; N, 5.98.

*Complex **IrF−L1**.* The dimeric complex **B** [**Ir(dfppy)$_2$Cl$_2$**] (31 mg, 0.026 mmol) was dissolved in dichloromethane (6 mL) and methanol (6 mL), and **L1** (39 mg, 0.055 mmol) was added as a solid. The mixture was heated at 60 °C during the night. The solution was cooled to room temperature and the solvent evaporated to dryness. The residue was dissolved in DMF (1 mL) and dropwise added through a pad of Celite into an aqueous solution of KPF_6 (500 mg in 20 mL of water). The precipitate was collected on paper and washed with water (3 × 100 mL). The complex was dried in air and was purified by column chromatography on alumina. The desired complex was eluted with a gradient of methanol (0−1%) in dichloromethane as mobile phase. The analytically pure complex **IrF−L1** was obtained as yellow powder by crystallization in a mixture of dichloromethane/diethylether (50 mg, 68%). ^{1}H NMR (($CD_3)_2$CO, 300 MHz): δ 5.72−5.83 (m, 4H), 6.72−6.81 (m, 2H), 7.19−7.32 (m, 5H), 7.41−7.44 (m, 2H), 7.53−7.58 (m, 2H), 7.75−7.77 (m, 2H), 7.86−7.92 (m, 2H), 8.03−8.09 (m, 3H), 8.20−8.22 (m, 2H), 8.35−8.40 (m, 4H), 8.89 (d, 2H, ^3J =8.9 Hz). EI-MS m/z: 1257.1 ([M − PF_6]$^+$, 100). Anal. Calcd for $C_{54}H_{30}F_4I_2IrN_4(PF_6)$ (Mr = 1401.83): C, 46.27; H, 2.16; N, 4.00. Found: C, 46.10; H, 2.01; N, 3.88.

*Complex **Ir−L1**.* The dimeric complex **A** [**Ir(dbpz)$_2$(Cl)$_2$**] (91 mg, 0.029 mmol) was dissolved in dichloromethane (6 mL) and methanol (6 mL), and **L1** (20 mg, 0.029 mmol) was added as a solid. The mixture was heated at 60 °C during the night. The solution was cooled to room temperature and the solvent evaporated to dryness. The residue was dissolved in DMF (1 mL) and dropwise added through a pad of Celite into an aqueous solution of KPF_6 (500 mg in 20 mL of water). The precipitate was collected on paper and washed with water (3 × 100 mL). The complex was dried in air and was purified by column chromatography on alumina. The desired complex was eluted with a gradient of methanol (0−1%) in dichloromethane as mobile phase. The analytically pure complex **Ir−L1** was obtained as yellow powder by crystallization in a mixture of dichloromethane/diethylether (15 mg, 34%). ^{1}H NMR (($CD_3)_2$CO, 300 MHz): δ 5.71 (s, 2H), 6.69−6.73 (m, 2H), 6.85 (dd, 1H, ^3J =7.6 Hz, ^4J =1.4 Hz), 7.15−7.20 (m, 3H), 7.28−7.34 (m, 2H), 7.41−7.56 (m, 8H), 7.84−7.93 (m, 6H), 7.97−8.09 (m, 2H), 8.14−8.20 (m, 4H), 8.32−8.45 (m, 4H), 8.62−8.66 (m, 2H), 8.76−8.83 (m, 2H), 9.37−9.43 (m, 2H). EI-MS m/z: 1435.1 ([M − PF_6]$^+$, 100). Anal. Calcd for $C_{72}H_{40}I_2IrN_6(PF_6)$ (Mr = 1580.12): C, 54.73; H, 2.55; N, 5.32 Found: C, 54.42; H, 2.88; N, 5.49.

*Complex **IrF−Os**.* The dimeric complex **B** [**Ir(dfppy)$_2$Cl$_2$**] (23 mg, 0.02 mmol) was dissolved in dichloromethane (6 mL) and methanol (6 mL), and **Os−L2** (39 mg, 0.055 mmol) was added as a solid. The mixture was heated at 60 °C during the night. The solution was cooled to room temperature and the solvent evaporated to dryness. The residue was dissolved in DMF (1 mL) and dropwise added through a pad of Celite into an aqueous solution of KPF_6 (750 mg in 20 mL of water). The precipitate was collected on paper and washed with water (3 × 100 mL). The complex was dried in air and was purified by column chromatography on alumina. The desired complex was eluted with a gradient of methanol (1−4%) in dichloromethane as mobile phase. The analytically pure complex **IrF−Os** was obtained as dark powder by recrystallization in a mixture of dichloromethane/diethylether (60 mg, 80%). ^{1}H NMR (($CD_3)_2$CO, 300 MHz): δ 5.73−5.83 (m, 4H), 6.72−6.80 (m, 4H), 7.14−7.32 (m, 5H), 7.41−7.59 (m, 10H), 7.72−7.76 (m, 1H), 7.86−8.10 (m, 16H), 8.19−8.21 (m, 2H), 8.31−8.39 (m, 4H), 8.77−8.80 (m, 5H), 8.86−8.89 (m, 2H). EI-MS m/z: 2103.2 ([M − PF_6]$^+$, 100), 979.1 ([M − 2PF_6]$^{2+}$, 30). Anal. Calcd for $C_{86}H_{53}F_4IIrN_{10}Os(PF_6)_3$ (Mr = 2246.65): C, 45.98; H, 2.38; N, 6.23. Found: C, 45.74; H, 2.17; N, 6.31.

*Complex **Ir**.* The dimeric complex **A** (84 mg, 0.054 mmol) was dissolved in dichloromethane (6 mL) and methanol (6 mL), and 5-ethynyl-2,2′-bipyridine (20 mg, 0.088 mmol) was added as a solid. The mixture was heated at 60 °C during the night. The solution was cooled to room temperature and the solvent evaporated to dryness. The residue was dissolved in DMF (1 mL) and dropwise added through a pad of Celite into an aqueous solution of KPF_6 (500 mg in 20 mL of water). The precipitate was collected on paper and washed with water (3 × 100 mL). The complex was dried in air and was purified by column chromatography on alumina. The desired complex was eluted with a gradient of methanol (0−1%) in dichloromethane as mobile phase. The analytically pure complex **Ir** was obtained as orange powder by crystallization in a mixture of dichloromethane/diethylether (20 mg, 35%). ^{1}H NMR (($CD_3)_2$CO, 300 MHz)): δ 3.95 (s, 1H), 6.62 (d, 1H, ^3J =7.6 Hz), 6.73 (d, 1H, ^3J =7.6 Hz), 7.12−7.21 (m, 2H), 7.44−7.57 (m, 5H), 7.78−8.01 (m, 6H), 8.11−8.24 (m, 4H), 8.32 (t, 2H, ^3J =7.9 Hz), 8.43 (d, 2H, ^3J =8.6 Hz), 8.68 (d, 2H, ^3J =8.6 Hz), 8.73−8.77 (m, 2H), 9.39−9.43 (m, 2H). ESI-MS (positive mode in CH_3OH/CH_2Cl_2) m/z: 931.4 ([M − PF_6]$^+$, 100). Anal. Calcd for $C_{52}H_{30}IrN_6(PF_6)$ (Mr = 1076.02): C, 58.04; H, 2.81; N, 7.81. Found: C, 58.12; H, 3.04; N, 7.62.

*Complex **IrF−Ir−Os**.* In a Schlenk tube, compounds **IrF−Os** (25 mg, 0.011 mmol) and complex **Ir** (14 mg, 0.013 mmol) were dissolved in a mixture of THF (2 mL), benzene (2 mL), and triethylamine (2 mL). Argon was bubbled through the mixture for 30 min, then [Pd(PPh$_3$)$_4$] (2 mg) was added and the mixture was stirred at 60 °C for 1 day. The solution was cooled to room temperature and the solvent evaporated to dryness. The residue was dissolved in DMF (1 mL) and dropwise added through a pad of Celite into an aqueous solution of KPF_6 (750 mg in 20 mL of water). The precipitate was collected on paper and washed with water (3 × 100 mL). The complex was dried in air and was purified by column chromatography on alumina. The desired complex was eluted with a gradient of methanol

dx.doi.org/10.1021/ic400809a | Inorg. Chem. 2013, 52, 8653−8664

Scheme 1[a]

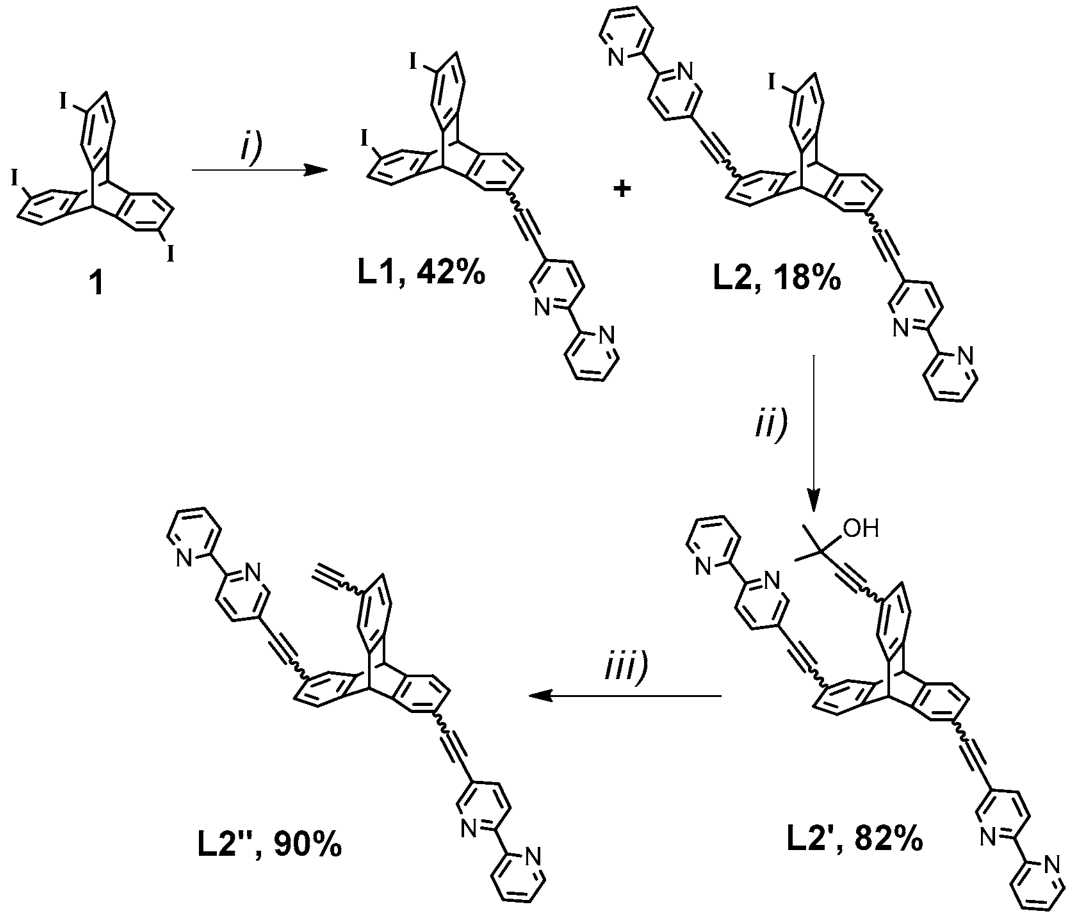

[a](i) 5-Ethynyl-2-2′-bipyridine, $[Pd(PPh_3)_2Cl_2]$, CuI, THF, Et_3N, room temperature; (ii) propargylic alcohol, $[Pd(PPh_3)_2Cl_2]$, CuI, THF, Et_3N, room temperature; (iii) benzene, NaOH. All ligands were prepared as mixture of regioisomers.

(1−4%) in dichloromethane as mobile phase. The complex **IrF−Ir−Os** was obtained as black powder by crystallization in a mixture of dichloromethane/diethylether (18 mg, 52%). ^{1}H NMR $(CD_3)_2CO$, 300 MHz): δ 5.74−5.76 (m, 2H), 5.81−5.84 (m, 2H), 6.70−6.79 (m, 4H), 7.15−7.27 (m, 8H), 7.43−7.57 (m, 15H), 7.74−7.78 (m, 3H), 7.90−8.06 (m, 24H), 8.09−8.23 (m, 5H), 8.34−8.45 (m, 8H), 8.63−8.66 (m, 2H), 8.78−8.90 (m, 8H), 9.38−9.40 (m, 1H). EI-MS m/z: 2906.4 ($[M - 2PF_6]^{2+}$, 100) 2761.5 ($[M - 3PF_6]^{3+}$, 30). Anal. Calcd for $C_{138}H_{82}F_4Ir_2N_{16}Os(PF_6)_4$ (Mr = 3196.75): C, 51.88; H, 2.59; N, 7.01. Found: C, 52.14; H, 2.79; N, 7.32.

■ RESULTS AND DISCUSSION

The schematic structures of ligands and complexes that are the focus of the present report are illustrated in Schemes 1−3 and are as follows: **L1** and **L2** (**L2′**, **L2″**) are two types of triptycene ligands, with different number of 5-ethynyl-2,2′-bipyridine (e-bipy) groups linked to the triptycene core through the rigid ethynylene spacer; **IrF**, **Ir**, and **Os** are Ir(III) and Os(II) monometallic complexes; **IrF−L1**, **Ir−L1**, and **Os−L2** are defined dyads, containing two photoactive subunits (i.e., a metal complex and the triptycene ligand, linked together through acetylide bridges); **IrF−Os** is a triad, with two metal complexes and the tritpycene bridging ligand; and **IrF−Ir−Os** is a tetrad, built up with three metal complexes and a triptycene unit. Model compounds for the study of the multichromophoric systems, triad and tetrad, are divided into two groups. The first group is composed of the bridging ligands **L1** and **L2″** and by the monometallic complexes **IrF**, **Ir**, and **Os**. The second group of models is composed of the three dyads **IrF−L1**, **Ir−L1**, and **Os−L2**. All of these proved to be suitable models for the interpretation of the photophysical features displayed by the multichromophoric arrays **IrF−Os** and **IrF−Ir−Os**.

Preparation of Ligands. The synthesis of ligands **L1** and **L2** is sketched in Scheme 1. The starting 2,6,14-triiodotriptycene[14] was allowed to react under smooth conditions with 5-ethynyl-2,2′-bipyridine (e-bipy)[28] leading to the monosubstituted e-bipy ligand **L1** in 42% yield and to the disubstituted e-bipy derivative **L2** in 18% yield. Under these conditions, the trisubstituted derivative was not isolated, and the starting triiodotriptycene was recovered and recycled. The residual iodo group in compound **L2** was converted to an ethynyl function to have an adequate reference compound for the spectroscopy, using a two-step protocol previously used on many occasions (Scheme 1).[29]

The preparation of the triptycene iridium(III) and osmium(II) complexes required the preparation of three heteroleptic starting complexes carrying in each case a 5-ethynyl-2,2′-bipyridine ligand for cross-coupling with the iodo-triptycene residues (Scheme 2). These iridium precursors are conveniently prepared from the known μ-dichloro dimers. One of the iridium complexes, **Ir**, has been constructed with dibenzo[a,c]-phenazine, dbpz,[30] a ligand known to generate highly colored complexes absorbing at low energy (Scheme 2).

Scheme 2[a]

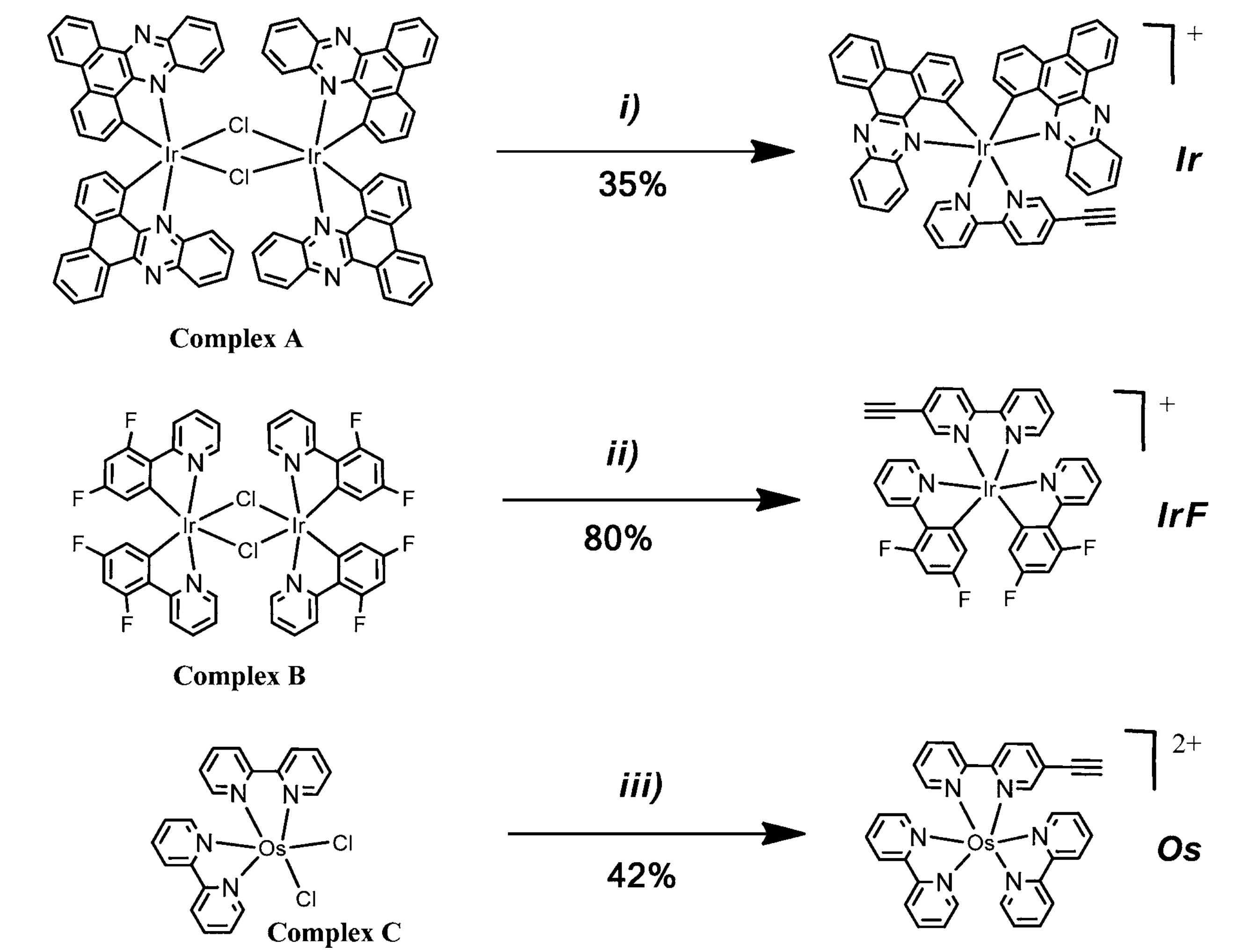

[a](i) 5-Ethynyl-2,2′-bipyridine (0.5 equiv), CH_2Cl_2/MeOH (2/1), 60 °C, 18 h; (ii) 5-ethynyl-2,2′-bipyridine (0.5 equiv), CH_2Cl_2/MeOH (2/1), 60 °C, 18 h; (iii) 5-ethynyl-2,2′-bipyridine (1.1 equiv), EtOH, microwave, 1200 W, 180 °C, 1 h.

The synthesis of the target complex and the intermediates is depicted in Scheme 3. Likewise, the preparation of the Os and Ir precursor and the preparation of **Os−L2** and **IrF−Os** complexes is straightforward using a step-by-step complexation of $[Os(bpy)_2Cl_2]$ and complex **B** in a second step. The two other reference complexes **IrF−L1** and **Ir−L1** were prepared in a similar manner using, respectively, complexes **B** and **A** in stoichiometric proportion. Finally, the most difficult synthesis was the cross-coupling between the mixed complex **IrF−Os** and **Ir**, providing the target heterotrinuclear complex **IrF−Ir−Os** in only 52% yield. Notice that the use of ligand **L2″** as a preorganized platform with preformed complexes, bearing a single 5-bromo-2,2′-bipyridine ligand and using Pd(0)-promoted coupling reactions, is not effective in our hands. All novel complexes have been characterized by NMR, UV−vis absorption spectroscopy, electrospray-mass, and elemental analysis, and all data unambiguously confirm the expected molecular structures drawn in Schemes 1−3 (see Experimental Section and Supporting Information).

Absorption. Absorption spectra for the compounds recorded in dilute solution ($c = 2 \times 10^{-5}$ M) at room temperature are displayed in Figures 1 and 2, and relevant data are collected in Table 1.

The spectral profiles of the ligands **L1** and **L2″**, recorded in CH_2Cl_2, show a specific intense absorption band in the near-UV region (λ_{max} = 346 nm, ε_{max} = 27 400 $M^{-1}{\cdot}cm^{-1}$ for **L1**, and λ_{max} = 327 nm, ε_{max} = 72 300 $M^{-1}{\cdot}cm^{-1}$ for **L2″**), originating from $^1\pi,\pi^*$ triptycene core transitions (Figure 1, Table 1).

Absorption spectra of the two Ir(III) complexes, **IrF** and **Ir**, recorded in CH_3CN like all other investigated complexes, are very different from each other (Figure 1, Table 1). The envelop of bands between 240 and 300 nm can be assigned to singlet spin-allowed ligand-centered (^{1}LC) transitions involving, at higher energy, the ppy ligands (ppy = 2-phenylpyridine) and, at lower energy, the bpy ligand (bpy = 2,2′-bipyridine).[31] In the case of **Ir**, the band related to the spin-permitted $^1\pi,\pi^*$ py-centered transition (py = pyridine or pyrazine), at λ_{max} = 251 nm and ε_{max} = 106 400 $M^{-1}{\cdot}cm^{-1}$, is more intense than the parent absorption band in **IrF** (λ_{max} = 247 nm, ε_{max} = 41 600 $M^{-1}{\cdot}cm^{-1}$) because of the larger conjugation of the 5-ring-fused dbpz system with respect to the ppy one. Weaker bands are observed in the spectral region between 350 and 550 nm and originate from spin-allowed transitions of mixed metal-to-ligand (^{1}MLCT) and ligand-to-ligand (^{1}LLCT) charge transfer character.[31] The low intensity tail extending at higher wavelengths present in both complexes (at λ > 400 and 580 nm for **IrF** and **Ir**, respectively) can be attributed to spin-

Scheme 3[a]

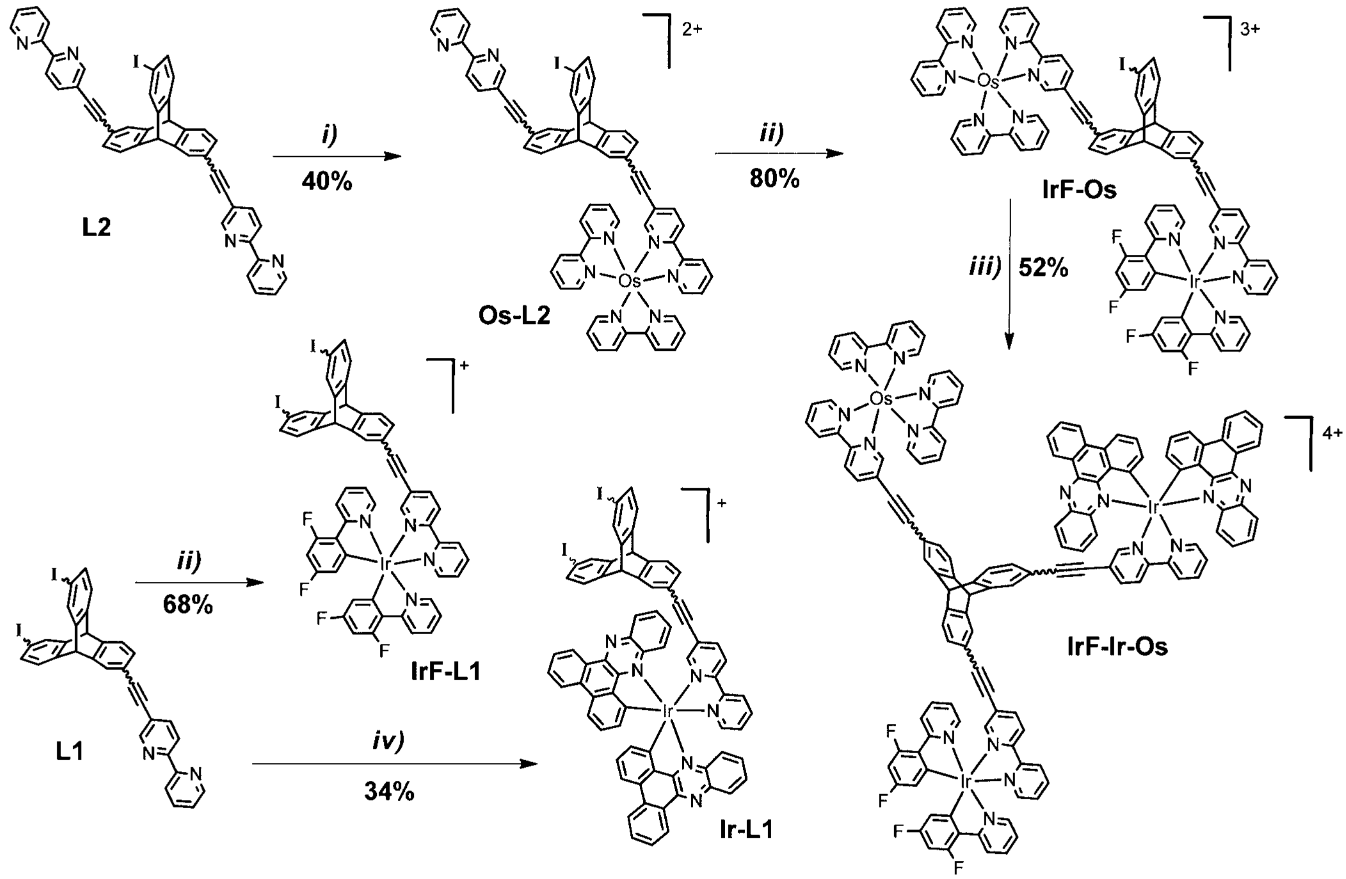

[a](i) $[Os(bpy)_2Cl_2]$ (1 equiv), EtOH, microwave, 1200 W, 180 °C, 1 h; (ii) complex B (0.5 equiv), CH_2Cl_2/MeOH (2/1), 60 °C, 18 h; (iii) complex Ir $[Pd(PPh_3)_4]$, $CH_3CN/Et_3N/C_6H_6$, 60 °C, 18 h; (iv) complex A (0.5 equiv), CH_2Cl_2/MeOH (2/1), 60 °C, 18 h. All complexes were prepared as a mixture of regioisomers.

forbidden ^{3}MLCT transitions. The presence of the iridium center results in a strong spin−orbit coupling (ζ_{Ir} = 3 909 cm^{-1}),[32] and the direct absorption from the singlet ground state to the triplet excited state becomes partially allowed.[33] In the absorption profile of the Os(II) complex, **Os**, it is possible to recognize (i) at 291 nm the typical intense (ε_{max} = 77 200 $M^{-1}\cdot cm^{-1}$) and narrow band of the $^1\pi,\pi^*$ bpy-centered transition (bpy = 2,2′-bipyridine) and (ii) at lower energy, the $d_{Os}\rightarrow\pi_{bpy}$ CT transition band, extended from 400 to 550 nm ($\varepsilon_{max} \approx$ 11 000 $M^{-1}\cdot cm^{-1}$).[34] The weak and broad band for **Os** that appears just like a tail in the range between 600 and 700 nm (Figure 1, Table 1) is associated with a formally spin-forbidden ^{3}MLCT set of transitions that is also, in this case, induced by the large spin−orbit coupling constant of the osmium metal (ζ_{Os} = 3 381 cm^{-1}).[32]

The absorption spectra of the second group of models, **IrF−L1**, **Ir−L1**, and **Os−L2** (Figure 1, bottom), can be interpreted on the basis of the features displayed by the units from which they originate (i.e., **IrF**, **Ir**, **Os**, **L1**, and **L2″**). Notably, in the spectral portion between 300 and 400 nm, a new band associated with an ^{1}LC triptycene absorption transition appears. This transition stems from the coordination by the metal center of the ethynylene-linked bpy site, which is otherwise unoccupied in the free ligands, **L1** and **L2″**, similarly to what was previously observed for a spirobifluorene-based system.[35] The spectrum of the dyads matches reasonably well the superposition of the spectra of the single components (Figure SI16); the only exception to an otherwise good superimposition is in the range between 300 and 400 nm, where the effect of new bpy−metal interactions introduces some distortions.

Absorption profiles of the investigated di- and trinuclear arrays, **IrF−Os** and **IrF−Ir−Os**, show bands due to the absorption of the subunits that comprise them (Figure 2). For both systems, moving from higher to lower energy, it is possible to observe (i) the band related to the $^1\pi,\pi^*$ py-centered transition of **IrF** and **Ir** subunits ($\lambda_{max} \approx$ 250 nm), (ii) the intense band typical of the $^1\pi,\pi^*$ bpy-centered transition ($\lambda_{max} \approx$ 300 nm), (iii) another band originating from the ^{1}LC triptycene absorption transition ($\lambda_{max} \approx$ 360 nm), (iv) a ^{1}CT transition band of lower intensity, extended from 400 to 550 nm, and (v) the tail for the ^{3} M_{Os}LCT transition, at λ > 600 nm. Figure 2 reports the spectra of the triad **IrF−Os** and the tetrad **IrF−Ir−Os** in comparison with the sum of subunits from which they are composed, taking into account the second group of model complexes (**IrF−L1**, **Ir−L1**, and **Os−L2**) and the relevant bridging ligands (**L1**, **L2″**). Both arrays display a good superimposition with the spectral sum of the single components, provided the contributions of the ligands **L1** and **L2″** are subtracted from the sum (dots in Figure 2), thus, indicating a weak ground-state electronic interaction between the satellite metal chromophores and the triptycene scaffold.

Emission. All examined complexes and ligands are luminescent at room temperature in air-equilibrated and

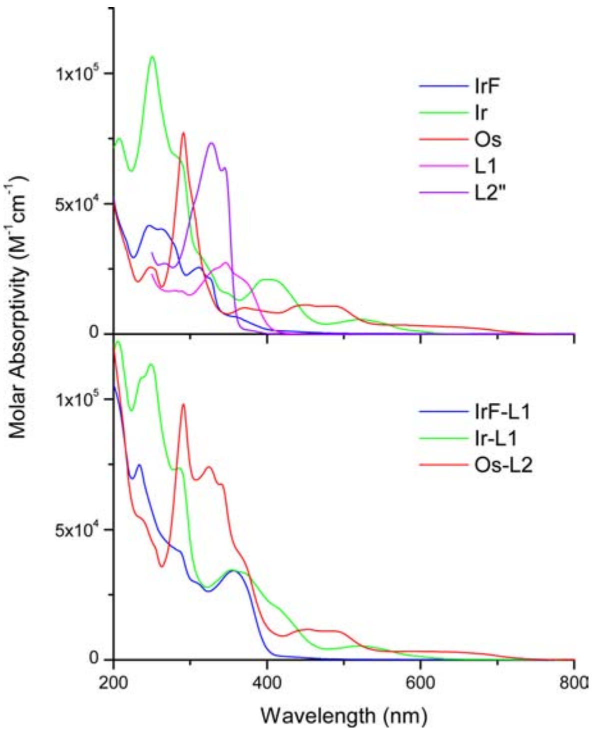

Figure 1. Absorption spectra of the triptycene ligands **L1** and **L2″** in CH_2Cl_2 and of the metal complexes **IrF**, **Ir**, and **Os** (top) and the dyads **IrF−L1**, **Ir−L1**, and **Os−L2** (bottom) in CH_3CN solution at room temperature.

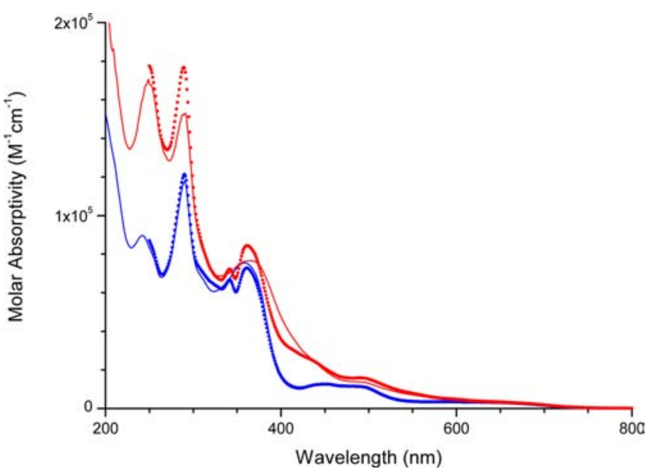

Figure 2. Absorption spectra of the triad **IrF−Os** (blue line) and the tetrad **IrF−Ir−Os** (red line) in CH_3CN. The dots represent the spectral addition of the absorption for the model components **IrF−L1**, **Ir−L1**, and **Os−L2**, corrected by the subtraction of the triptycene ligands contribution for **L1** and **L2″**.

deaerated solutions and at 77 K in glassy solutions; the relevant luminescence properties are summarized in Table 2. The room temperature luminescence profiles for ligands **L1**, **L2″** and for iridium and osmium complexes observed at room temperature in deaerated solutions (CH_2Cl_2 for ligands and CH_3CN for complexes) are illustrated in Figure 3, rescaled according to the corresponding photoluminescence quantum yields. The luminescence spectra recorded at 77 K in CH_2Cl_2/CH_3OH (1:1) frozen mixtures are displayed in Figure 4.

Both ligands **L1** and **L2″** show an intense short-living fluorescence in solution (ϕ = 0.37, 0.56 and τ = 1.9, 0.8 ns, respectively) peaking around 380 nm, only slightly blue-shifted at 77 K (λ_{max} = 360, 380 nm, Table 2). Interestingly, at low temperature in frozen solution both **L1** and **L2″** show a characteristic phosphorescence emission (τ = 145 and 166 ms, respectively, Table 2 and Figure 4) with a well-resolved vibronic structure. From the highest energy phosphorescence peak, an energy level of ≈ 2.43 eV can be evaluated for the lowest triplet excited state of both ligands.

The luminescence properties of **Os** are easily identified as having a ^{3}MLCT nature upon comparison with literature data and when observing the blue shift of the luminescence maximum in the transition from solution to glassy matrix at 77 K.[36] In fact, for CT emitters dissolved in polar solvents, the reorientation of solvent dipoles is prevented on passing from a fluid to a frozen environment, thus hindering the stabilization of the CT state. Notice that the emission peak exhibited by **Os** lies at lower energy than for $[Os(bpy)_3]^{2+}$ by ≈ 930 cm^{-1}. This occurrence might explain the lower quantum yield and shorter lifetime observed for **Os** ($\phi = 1 \times 10^{-3}$ and τ = 16.0 ns, Table 2) with respect to the parent compound, possibly based on energy gap law effects.[37] For the mononuclear Ir(III) complexes, the complex with fluorinated ppy, **IrF**, shows a blue shift of the emission maxima at room temperature and 77 K, a comparable quantum yield and shorter lifetime, with respect to the dbpz derivative **Ir** (Table 2). The latter shows a remarkably high efficiency as a red emitter at room temperature in deaerated solvent (λ_{max} = 660 nm and ϕ = 0.23, Table 2). In both cases at low temperature, the emission band moves to higher energies with respect to that at room temperature by 2640 and 800 cm^{-1} for **IrF** and **Ir**, respectively. Also in this case, the photophysical behavior is consistent with a ^{3}CT character of the emission, as further supported by the calculated values of the radiative constants for **IrF** and **Ir**, $k_r = 2.9 \times 10^5$ and 1.8×10^5 s^{-1} ($k_r = \phi/\tau$), respectively.[31] In the case of complex **IrF**, the observed emission band can be assigned to the $d_{Ir} \rightarrow \pi_{bpy}$ transition, originating from the orbitals mainly centered on the metal and the cyclometalating ligand and ending on the bpy-centered orbitals ($ML_{bpy}CT$).[38] The similar radiative constant calculated for **Ir** might indicate that the observed transition originates from the same $ML_{bpy}CT$ excited state, with the LUMO orbital mainly located on the bpy moiety of the complex (Table 2).

The introduction of the triptycene unit attached to the bpy ligand in **IrF−L1**, **Ir−L1**, and **Os−L2** induces some modifications on the photophysical behavior of the complexes. In particular, in the case of **IrF−L1**, the photoluminescence quantum yield in solution is decreased by ≈ 70% with respect to the parent compound **IrF**, and a concomitant increase of the excited state lifetime is observed (τ = 4.35 and 0.86 μs for **IrF−L1** and **IrF**, respectively). On the other end, the emission spectrum of **IrF−L1** shows a structured profile at room temperature (Figure 4, bottom) and its maximum is blue-shifted by only 410 cm^{-1} on going from fluid to rigid solution. All these data indicate a more pronounced ^{3}LC character of the **IrF−L1** emitting state, which was confirmed by the low value calculated for the radiative constant, $k_r = 1.7 \times 10^4$ s^{-1}.[31] It should be noted that the triplet energy level calculated from the emission maximum at 77 K for **IrF−L1** (E_T = 2.32 eV) is comparable to that of the triptycene triplet (E_T = 2.43 eV, see discussion above). Thus, the longer lifetime observed for **IrF−L1** with respect to **IrF** might be due to an involvement of the triplet levels centered on the triptycene ligand. Complexes **Ir−L1** and **Os−L2** seem to be less affected by the introduction of

Table 1. Absorption Properties of Ligands and Complexes[a]

	λ_{max}, nm (ε_{max}, $M^{-1}\cdot cm^{-1}$)
L1	335 sh (25200), 346 (27400), 370 sh (20700)
L2″	327 (72300), 345 (63800)
IrF	247 (41600), 312 (25600)
Ir	251 (106400), 400 (20900), 519 (5600)
Os[b]	291 (77200), 449 (11900), 482 (11000), 580 (3900)
IrF−L1	234 (74800), 287 sh (41500), 355 (34200)
Ir−L1	249 (113500), 286 sh (73500), 354 (34500), 520 (5400)
Os−L2	291 (98100), 324 (74000), 455 (11700), 635 (3000)
IrF−Os	242 (89600), 289 (117000), 358 (75500), 452 (12300)
IrF−Ir−Os	249 (170600), 291 (153000), 363 (76500), 491 sh (13800)

[a]In CH_2Cl_2 for ligands and CH_3CN for complexes, at room temperature. [b]From ref 8b.

Table 2. Luminescence Properties of Ligands and Complexes[a]

	rt			77 K	
	λ_{max}, nm	ϕ^a	τ, ns[b]	λ_{max}, nm	τ, μs[c]
L1	383, 455	0.37	1.9	362, 380	
				509, 545[d]	145×10^3
L2″	380	0.56	0.8	363, 379	
				512, 550[d]	166×10^3
IrF	564	0.25 (0.045)	860 (173)	491, 530, 573	5.2
Ir	660	0.23 (0.032)	1300 (254)	626	20.2
Os[e]	798	0.001	16	736	2.3
IrF−L1	547	0.073 (0.007)	4350 (373)	535, 580, 620	5.8
Ir−L1	664	0.177 (0.023)	2020 (258)	627	19.2
Os−L2	804	0.001 (0.001)	39	732	0.9
IrF−Os	804	0.001 (0.001)	30	736	n.d.
IrF−Ir−Os	770	0.001 (0.001)	30 (30)	758	n.d.

[a]In deaerated and air-equilibrated (in parentheses) solutions, CH_2Cl_2 for ligands and CH_3CN for complexes. λ_{exc} = 340 nm for ligands, 355 nm for **Ir**, **IrF**, and **Os**, 450 nm for **IrF−L1**, 470 nm for **Ir−L1**, 600 nm for **Os** and **Os−L2**. n.d. is not detected or weak signal. [b]λ_{exc} = 331 nm for ligands, 373 nm for **IrF** and **Ir**, 465 nm for **IrF−L1**, **Ir−L1**, **Os**, and **Os−L2**. [c]λ_{exc} = 370 nm for **Ir** and **IrF**, 465 nm for **IrF−L1** and **Ir−L1**, 465 nm for **Os−L2**. [d]Phosphorescence data for ligands are obtained with pulsed lamp, λ_{exc} = 340 nm. [e]From ref 8b.

the triptycene ligand and maintain the emission features typical of the relevant precursors **Ir** and **Os**. **Ir−L1** displays an emission centered at 664 nm with an almost identical quantum yield and lifetime with respect to **Ir** (Table 2), indicating that the emitting state is the CT triplet centered on the Ir unit. **Os−L2** shows the typical features of **Os** MLCT phosphorescence with slightly improved properties with respect to the model **Os**; the emission quantum yield is moderately higher and the lifetime longer (Table 2).

Transient Absorption. In order to deeply investigate the nature of the excited states in the Ir-containing dyads, **Ir−L1** and **IrF−L1**, laser flash photolysis experiments have been performed for the two dyads and the respective models **Ir**, **IrF**, and **L1**. Ligand **L2″** has also been investigated for comparison purposes with respect to **L1**. Transient absorption spectra of ligand **L1** in deaerated CH_2Cl_2 and complexes **Ir**, **IrF−L1**, and **Ir−L1** in deaerated CH_3CN detected upon excitation at 355 nm are reported in Figure 5. Ligand **L1** shows a broad and intense difference absorption spectrum that peaks at 470 and 520 nm (Figure 5), whereas ground-state bleaching features are noted below 370 nm. Single-exponential decays are registered at any wavelength with a measured lifetime of 4.6 μs in deaerated solvent. Ligand **L2″** shows very similar spectral features and a lifetime of 7.4 μs (Figure SI17). The observed spectra can be assigned to the lowest-lying π,π^* triplet state of the triptycene ligands. **Ir** and **IrF** spectra are characterized by ground-state bleaching features that sum with absorption in the 350−500 nm region; for **IrF**, whose ground-state absorption is confined below 370 nm (Figure 1), a clearer visualization of intense transient absorption with maxima at 400 and 470 nm is feasible (Figure SI18). The region up to 700 nm is then dominated by emission features (cf. Figure 3 and Table 2), and in the region above 750 nm, a weak absorption tail emerges. The measured lifetimes are 1.4 μs and 760 ns for **Ir** and **IrF**, respectively, in good agreement with the luminescence lifetimes (Table 2). The observed spectra are thus undoubtedly ascribed to the MLCT triplet excited state of the Ir complexes.[39] The spectra of the **Ir−L1** and **IrF−L1** dyads are markedly different from each other (Figure 5); whereas **Ir−L1** shows the typical features of ^{3}MLCT absorption observed for **Ir**, the spectrum of **IrF−L1** is different from that of its parent model **IrF**, and it clearly exhibits the features observed for ligand **L1**, showing a broad absorption profile that peaks at 440 and 530 nm. The measured lifetimes of 1.6 and 4.7 μs for **Ir−L1** and **IrF−L1**, respectively, support the comparison. These data thus confirm the LC nature of the lowest-lying triplet excited state of dyad **IrF−L1**, already speculated on the basis of the luminescence data.

Energy Transfer. On the basis of the absorption data, the component units in the arrays **IrF−Os** and **IrF−Ir−Os** can be considered as weakly interacting and can be separately addressed in the analysis of the systems. Based on this assumption, it is possible to draw the layout of the excited states as obtained by the estimation of the energies from the emission

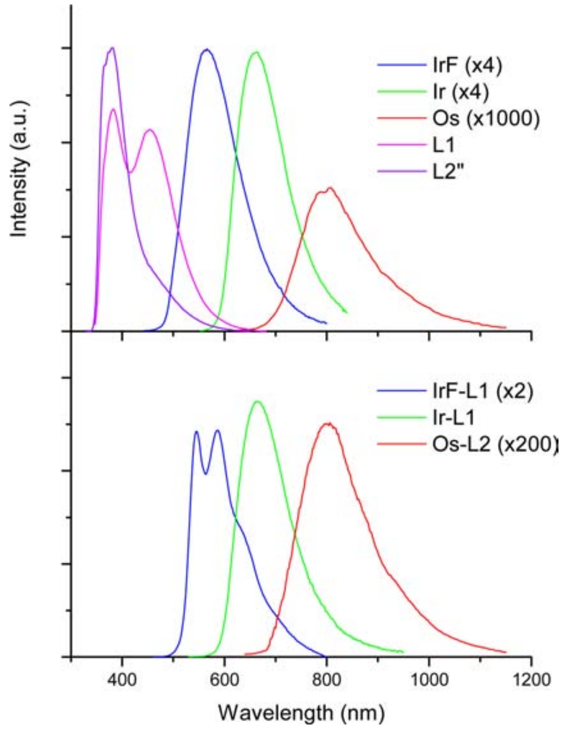

Figure 3. Room temperature-corrected emission spectra of the ligands **L1** and **L2″** in deaerated CH_2Cl_2 solution and of the model metal complexes, **IrF**, **Ir**, and **Os** in deaerated CH_3CN solution (top), and of the dyads **IrF−L1**, **Ir−L1**, and **Os−L2** in deaerated CH_3CN solutions (bottom). Spectral areas are scaled proportional to the quantum yields.

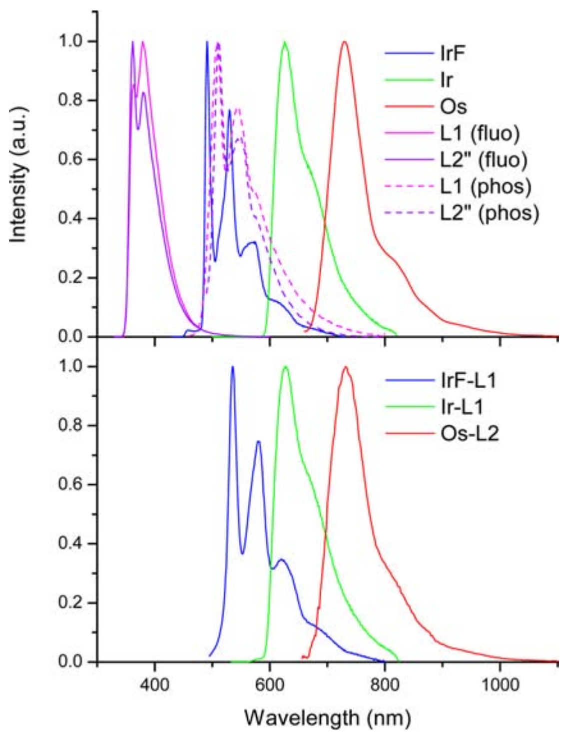

Figure 4. Normalized-corrected emission spectra at 77 K in CH_3OH/CH_2Cl_2 (1:1 v/v) glassy solutions of the triptycene ligands **L1** and **L2″** (fluorescence, full line, and phosphorescence, dotted line), the model complexes **IrF**, **Ir**, and **Os** (top) and dyads **IrF−L1**, **Ir−L1**, and **Os−L2** (bottom).

maxima observed at 77 K for the **L1/L2″** ligands, **IrF**, **Ir**, and **Os** model complexes. The resulting energy levels diagram is shown in Scheme 4. The triptycene ligand triplet level has been calculated from the maximum in the phosphorescence spectrum of **L1/L2″**, while the metal-based singlet energy levels have been estimated from the onset of the lowest energy ^{1}MLCT absorption band of model **IrF**, **Ir**, and **Os** complexes. From Scheme 4, it appears that the triptycene ligand has the highest energy content (3.42 eV for S_1); the energy transfer processes from this state to the metal-based singlet levels are exoergonic by 0.34, 0.72, and 1.12 eV (from **L1/L2″** to **IrF**, **Ir**, and **Os**, respectively). It should also be noted that the $^3\pi,\pi^*$ and ^{3}LC/^{3}MLCT levels of triptycene and **IrF** are almost isoenergetic (vide supra). From inspection of the absorption spectra of the model systems and of the arrays, **IrF−Os** and **IrF−Ir−Os**, it is not possible to identify a set of selected wavelengths yielding distinct excitation of the components. Only the selective excitation of the Os-based units can be achieved on the ^{3}MLCT band at $\lambda > 600$ nm, and this serves as useful reference. Thus, to get insight into the cascade of photoinduced processes in the multichromophoric arrays, we have run multiexcitation emission map experiments, spanning the excitation range between 240 and 330 nm (i.e., the spectral region of predominant triptycene absorption), and reading the emission in the spectral range 340−820 nm, where the residual emission of the components together with the sensitized emission of the final Os energy collector could be observed. The emission maps obtained in deaerated acetonitrile solution for the triad **IrF−Os** and the tetrad **IrF−Ir−Os** are reported in Figures 6 and 7 (the maps for dyads **IrF−L1**, **Ir−L1**, and **Os−L2** are reported in Figures SI19−SI21). Here, no residual emission can be observed in the spectral range 340−600 nm, indicating that the luminescence from the triptycene and **IrF** units is almost completely quenched. On the other end, upon excitation of the **IrF−Ir−Os** tetrad between 240 and 270 nm, an emission ascribable to the excited states located on the **Ir** unit is observed, with an intensity comparable to that of the Os-based luminescence. Taking into consideration the large difference in photoluminescence quantum yield between **Ir** and **Os**, the observed weak emission has to be ascribed to the residual emission from the Ir unit, as a result of the quenching by the Os unit. Ultimately, in both **IrF−Os** and **IrF−Ir−Os**, the most intense signal (above 750 nm) originates from the Os-based excited state either from direct excitation or by transfer of energy from the other units in the array.

From time-resolved luminescence analysis of **IrF−Os** and **IrF−Ir−Os**, lifetimes of 5 and 18 ns for the residual emission of the IrF and Ir units, respectively, have been detected. These values account for energy transfer rate constants, calculated as $k_{EnT} = \tau_q^{-1} - \tau^{-1}$, of 1.9×10^8 s^{-1} and 5.2×10^7 s^{-1} for the IrF→Os and Ir→Os process, with efficiencies $\eta_{EnT} = 1 - \tau_q/\tau$ of 0.97 and 0.93, respectively (Table SI1). By using the available spectroscopic properties and the formalism developed by Förster for a through-space dipole−dipole interaction energy transfer mechanism it is possible to calculate the overlap integral J_F and the critical radius R_0 (see Supporting Information). Considering a donor−acceptor separation d = 19 Å estimated from molecular modeling of the arrays **IrF−Os** and **IrF−Ir−Os**, the values for $J_F \sim 3.8 \times 10^{-14}$ and 3.2×10^{-14} cm^3·M^{-1} and $R_0 < 16$ Å are obtained by applying the Förster model, with energy transfer rate constants lower by ≈1 order of magnitude with respect to the experimental values (Table SI2). Thus, this analysis seems to rule out a major contribution from

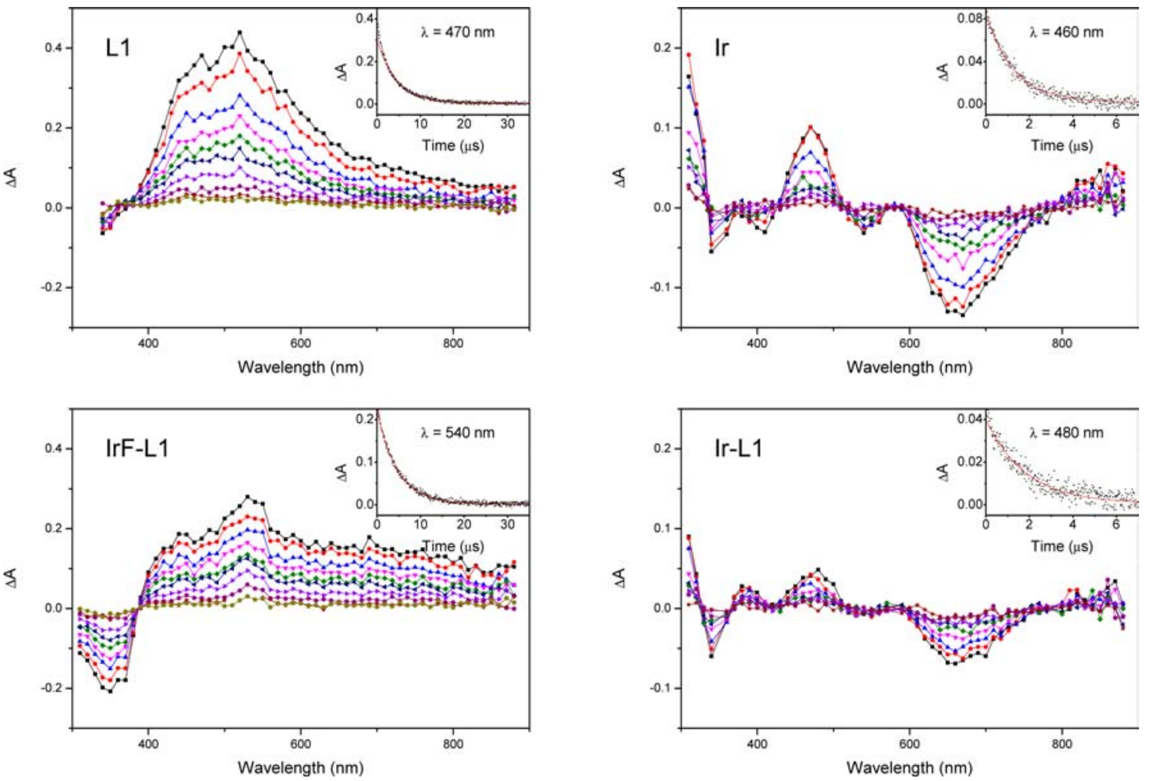

Figure 5. Transient absorption spectra of **L1** in deaerated CH_2Cl_2 and of **Ir**, **IrF−L1**, and **Ir−L1** in deaerated CH_3CN at incremental delay times (0−15.0 μs for **L1** and **IrF−L1**, 0−3.5 μs for **Ir** and **Ir−L1**). λ_{exc} = 355 nm, A_{355} = 0.52, 3.1 mJ/pulse. Time evolutions at selected wavelengths and monoexponential fitting of the decays are shown in the insets.

Scheme 4. Energy Level of the Excited States with Respect to the Ground State

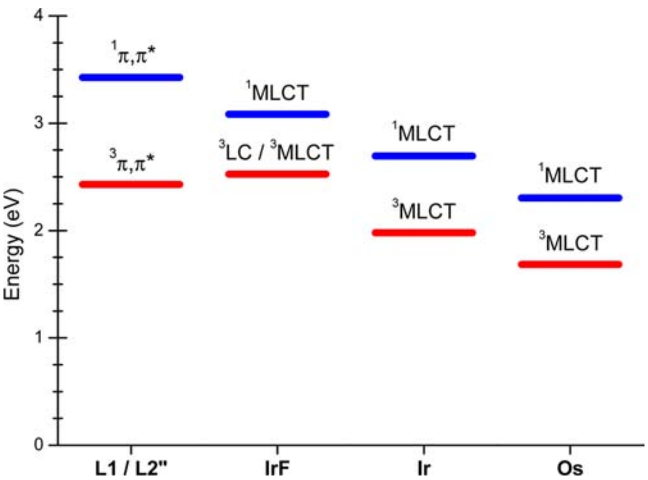

the dipole−dipole interaction mechanism in the observed photoinduced energy transfer processes. In a similar way, an overlap integral $J_D \sim 5 \times 10^{-5}$ and 2.5×10^{-5} cm within a bridge-mediated double-electron-exchange model is calculated for the IrF→Os and Ir→Os processes, respectively. This would require a small electronic-coupling term H ∼ 1.8 and 1.3 cm^{-1} (Table SI3), respectively, to account for the energy transfer rate constants derived from experimental data, compatible with through-bond interaction in systems connected with aromatic bridges. It should be noted that the triplet emission from both iridium donors, **IrF** and **Ir**, largely overlaps with the direct ^{3}MLCT absorption band of the osmium unit and the process can be considered mainly as a triplet-to-triplet energy transfer. In this case, the Dexter-type mechanism is prevailing over the dipole−dipole interaction mechanism on the basis of the selection rules, as also confirmed by our calculations.

■ CONCLUSION

In summary, here we have synthesized and investigated the photophysical properties of a series of new Ir−Os supramolecular assemblies, with the photoactive units at fixed positions diverging from a central triptycene scaffold in a star-shaped arrangement. The synthesis of the multichromophoric arrays goes through the preparation of three heteroleptic Ir(III) and Os(II) starting complexes carrying in each case a 5-ethynyl-2,2′-bipyridine ligand for cross-coupling with the iodo-triptycene residues. The most difficult synthetic step was the final cross-coupling between the mixed complex **IrF−Os** and **Ir** providing the target heterotrinuclear complex **IrF−Ir−Os**. Fast and efficient energy transfer processes leading to the final population of the Os-based triplet level starting from the triptycene singlet and Ir-based triplets have been observed from luminescence investigation. Transient absorption measurements allowed us to highlight the different nature of the excited states in the Ir-containing dyads and the role of the low-lying triplet level of the triptycene scaffold in it.

These outcomes clearly show that the triptycene framework can be successfully employed in the construction of rigid star-shaped antenna systems, and they highlight its behavior as an active component in the energy cascade. This basic understanding might be useful in the design of new light collectors in optoelectronic devices and energy conversion systems.

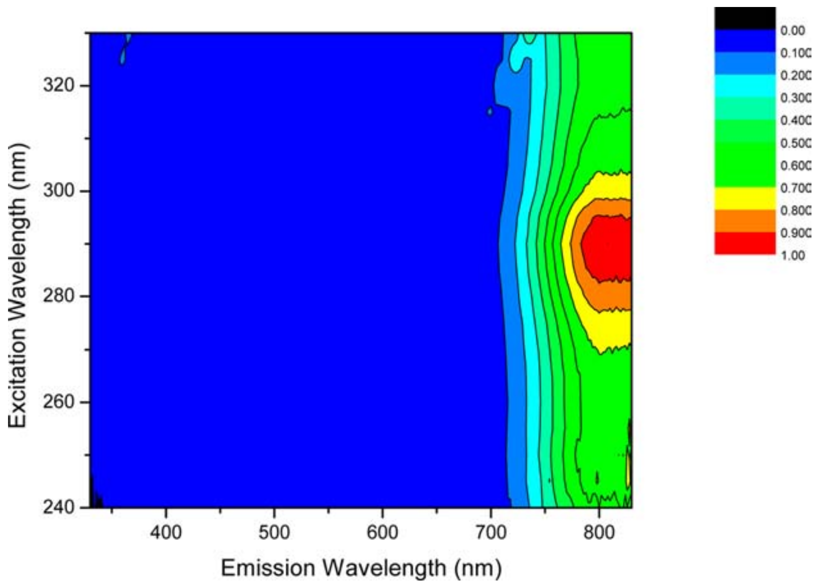

Figure 6. Map of normalized **IrF−Os** luminescence in CH_3CN at room temperature.

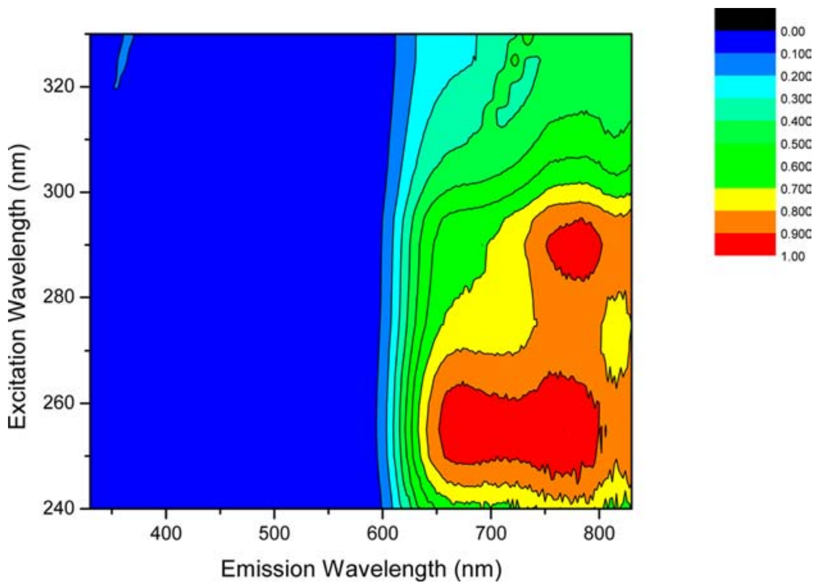

Figure 7. Map of normalized **IrF−Ir−Os** luminescence in CH_3CN at room temperature.

■ ASSOCIATED CONTENT

Supporting Information

General methods, NMR traces, and experimental details on photophysics. This material is available free of charge via the Internet at http://pubs.acs.org.

■ AUTHOR INFORMATION

Corresponding Author

*E-mail: ziessel@unistra.fr (R. Z.), andrea.barbieri@isof.cnr.it (A. B.).

Notes

The authors declare no competing financial interest.

■ ACKNOWLEDGMENTS

We thank the ESF-EUROCORES 10-EuroSolarFuels-FP-006 “Modular design of a bioinspired tandem cell for direct solar-to-fuel conversion” (SOLARFUELTANDEM) and the Italian CNR PM.P04.010 “Materiali Avanzati per la Conversione di Energia Luminosa” (MACOL) projects for financial support, and Mr. Giorgio Longino for technical assistance in the customization of the photophysical setup. We also warmly thank Johnson Matthey PLC for the loan of precious metals and the Centre National de la Recherche Scientifique (CNRS in France) for hosting the research.

■ REFERENCES

(1) (a) Balzani, V.; Bergamini, G.; Campagna, S.; Puntoriero, F. *Top. Curr. Chem.* **2007**, *280*, 1−36. (b) Balzani, V.; Credi, A.; Venturi, M. *ChemSusChem* **2008**, *1*, 26−58. (c) Hasobe, T. *Phys. Chem. Chem. Phys.* **2010**, *12*, 44−57. (d) Ward, M. D.; Barigelletti, F. *Coord. Chem. Rev.* **2001**, *216*, 127−154.

(2) (a) Muro, M. L.; Rachford, A. A.; Wang, X. H.; Castellano, F. N. *Top. Organomet. Chem.* **2010**, *29*, 159−191. (b) Rausch, A. F.; Homeier, H. H. H.; Yersin, H. *Top. Organomet. Chem.* **2010**, *29*, 193−235. (c) Williams, J. A. G. *Top. Curr. Chem.* **2007**, *281*, 205−268.

(3) (a) Kalinowski, J.; Fattori, V.; Cocchi, M.; Williams, J. A. G. *Coord. Chem. Rev.* **2011**, *255*, 2401−2425. (b) Ziessel, R.; Harriman, A. *Chem. Commun.* **2011**, *47*, 611−631.
(4) Alstrum-Acevedo, J. H.; Brennaman, M. K.; Meyer, T. J. *Inorg. Chem.* **2005**, *44*, 6802−6827.
(5) (a) Guillo, P.; Hamelin, O.; Batat, P.; Jonusauskas, G.; McClenaghan, N. D.; Menage, S. *Inorg. Chem.* **2012**, *51*, 2222−2230. (b) Nitadori, H.; Takahashi, T.; Inagaki, A.; Akita, M. *Inorg. Chem.* **2012**, *51*, 51−62.
(6) (a) Albrecht, M.; van Koten, G. *Angew. Chem., Int. Ed.* **2001**, *40*, 3750−3781. (b) Demas, J. N.; DeGraff, B. A. *Coord. Chem. Rev.* **2001**, *211*, 317−351.
(7) (a) Ardo, S.; Meyer, G. J. *Chem. Soc. Rev.* **2009**, *38*, 115−164. (b) Grätzel, M. *Inorg. Chem.* **2005**, *44*, 6841−6851. (c) Li, G. C.; Ray, L.; Glass, E. N.; Kovnir, K.; Khoroshutin, A.; Gorelsky, S. I.; Shatruk, M. *Inorg. Chem.* **2012**, *51*, 1614−1624.
(8) (a) Diring, S.; Ziessel, R.; Barigelletti, F.; Barbieri, A.; Ventura, B. *Chem.—Eur. J.* **2010**, *16*, 9226−9236. (b) Ventura, B.; Barbieri, A.; Barigelletti, F.; Diring, S.; Ziessel, R. *Inorg. Chem.* **2010**, *49*, 8333−8346.
(9) (a) Gust, D.; Moore, T. A.; Moore, A. L. *Acc. Chem. Res.* **2001**, *34*, 40−48. (b) Gust, D.; Moore, T. A.; Moore, A. L. *Acc. Chem. Res.* **2009**, *42*, 1890−1898. (c) Terazono, Y.; Kodis, G.; Liddell, P. A.; Garg, V.; Moore, T. A.; Moore, A. L.; Gust, D. *J. Phys. Chem. B* **2009**, *113*, 7147−7155.
(10) Oosterom, G. E.; Reek, J. N. H.; Kamer, P. C. J.; van Leeuwen, P. *Angew. Chem., Int. Ed.* **2001**, *40*, 1828−1849.
(11) Shunmugam, R.; Tew, G. N. *Macromol. Rapid Commun.* **2008**, *29*, 1355−1362.
(12) (a) Chong, J. H.; MacLachlan, M. J. *Chem. Soc. Rev.* **2009**, *38*, 3301−3315. (b) Jiang, Y.; Chen, C. F. *Eur. J. Org. Chem.* **2011**, 6377−6403.
(13) (a) Chong, J. H.; MacLachlan, M. J. *Inorg. Chem.* **2006**, *45*, 1442−1444. (b) Norvez, S. *J. Org. Chem.* **1993**, *58*, 2414−2418. (c) Zhang, C.; Chen, C. F. *J. Org. Chem.* **2007**, *72*, 9339−9341.
(14) Zhang, C.; Chen, C. F. *J. Org. Chem.* **2006**, *71*, 6626−6629.
(15) Karlen, S. D.; Godinez, C. E.; Garcia-Garibay, M. A. *Org. Lett.* **2006**, *8*, 3417−3420.
(16) Han, T.; Zong, Q. S.; Chen, C. F. *J. Org. Chem.* **2007**, *72*, 3108−3111.
(17) Zhang, C.; Chen, C. F. *J. Org. Chem.* **2007**, *72*, 3880−3888.
(18) Azerraf, C.; Cohen, S.; Gelman, D. *Inorg. Chem.* **2006**, *45*, 7010−7017.
(19) Sundermeier, M.; Zapf, A.; Mutyala, S.; Baumann, W.; Sans, J.; Weiss, S.; Beller, M. *Chem.—Eur. J.* **2003**, *9*, 1828−1836.
(20) Chou, H. H.; Shih, H. H.; Cheng, C. H. *J. Mater. Chem.* **2010**, *20*, 798−805.
(21) Beyeler, A.; Belser, P. *Coord. Chem. Rev.* **2002**, *230*, 29−39.
(22) Wasielewski, M. R.; Niemczyk, M. P.; Svec, W. A.; Pewitt, E. B. *J. Am. Chem. Soc.* **1985**, *107*, 5562−5563.
(23) Goldsmith, R. H.; Vura-Weis, J.; Scott, A. M.; Borkar, S.; Sen, A.; Ratner, M. A.; Wasielewski, M. R. *J. Am. Chem. Soc.* **2008**, *130*, 7659−7669.
(24) Gu, X. W.; Lai, Y. H. *Org. Lett.* **2010**, *12*, 5200−5203.
(25) (a) Ghanem, B. S.; Hashem, M.; Harris, K. D. M.; Msayib, K. J.; Xu, M. C.; Budd, P. M.; Chaukura, N.; Book, D.; Tedds, S.; Walton, A.; McKeown, N. B. *Macromolecules* **2010**, *43*, 5287−5294. (b) Long, T. M.; Swager, T. M. *Adv. Mater.* **2001**, *13*, 601−604.
(26) Tovar, J. D.; Rose, A.; Swager, T. M. *J. Am. Chem. Soc.* **2002**, *124*, 7762−7769.
(27) (a) Long, T. M.; Swager, T. M. *J. Am. Chem. Soc.* **2002**, *124*, 3826−3827. (b) Zhu, Z. G.; Swager, T. M. *J. Am. Chem. Soc.* **2002**, *124*, 9670−9671.
(28) Grosshenny, V.; Romero, F. M.; Ziessel, R. *J. Org. Chem.* **1997**, *62*, 1491−1500.
(29) Harriman, A.; Mallon, L.; Ziessel, R. *Chem.—Eur. J.* **2008**, *14*, 11461−11473.
(30) Konno, H. Iridium Complex and Luminous Material Using the Same. JP2005298483, 2005.
(31) Flamigni, L.; Barbieri, A.; Sabatini, C.; Ventura, B.; Barigelletti, F. *Top. Curr. Chem.* **2007**, *281*, 143−203.
(32) Montalti, M.; Credi, A.; Prodi, L.; Gandolfi, M. T. *Handbook of Photochemistry*, 3rd ed.; CRC Press, Taylor & Francis: Boca Raton, FL, 2006.
(33) Costa, R. D.; Monti, F.; Accorsi, G.; Barbieri, A.; Bolink, H. J.; Orti, E.; Armaroli, N. *Inorg. Chem.* **2011**, *50*, 7229−7238.
(34) Ventura, B.; Barbieri, A.; Barigelletti, F.; Seneclauze, J. B.; Retailleau, P.; Ziessel, R. *Inorg. Chem.* **2008**, *47*, 7048−7058.
(35) Ventura, B.; Barbieri, A.; Degli Esposti, A.; Seneclauze, J. B.; Ziessel, R. *Inorg. Chem.* **2012**, *51*, 2832−2840.
(36) Kumaresan, D.; Shankar, K.; Vaidya, S.; Schmehl, R. H. *Top. Curr. Chem.* **2007**, *281*, 101−142.
(37) Kober, E. M.; Caspar, J. V.; Lumpkin, R. S.; Meyer, T. J. *J. Phys. Chem.* **1986**, *90*, 3722−3734.
(38) Costa, R. D.; Orti, E.; Bolink, H. J.; Monti, F.; Accorsi, G.; Armaroli, N. *Angew. Chem., Int. Ed.* **2012**, *51*, 8178−8211.
(39) Wang, X. Y.; Prabhu, R. N.; Schmehl, R. H.; Weck, M. *Macromolecules* **2006**, *39*, 3140−3146.